Crosslinkable Hole-Transport Layer on Conducting Polymer for High-Efficiency White Polymer Light-Emitting Diodes

ARTICLE *in* ADVANCED MATERIALS · JANUARY 2007

Impact Factor: 17.49 · DOI: 10.1002/adma.200502769

8 AUTHORS, INCLUDING:

Melvin T Zin
University of Washington Seattle
16 PUBLICATIONS **354** CITATIONS

SEE PROFILE

Yun Chi
National Tsing Hua University
342 PUBLICATIONS **10,794** CITATIONS

SEE PROFILE

ADVANCED MATERIALS

DOI: 10.1002/adma.200502769

Crosslinkable Hole-Transport Layer on Conducting Polymer for High-Efficiency White Polymer Light-Emitting Diodes**

By *Yu-Hua Niu*, *Michelle S. Liu*, *Jae-Won Ka*, *Julie Bardeker*, *Melvin T. Zin*, *Richard Schofield*, *Yun Chi*, and *Alex K.-Y. Jen**

Organic and polymer light-emitting diodes (LEDs) have been the subject of intensive investigation in recent years because of their potential as emissive elements for flat-panel displays and white-light sources for general lighting. As dual-injection devices, multilayer structures with discrete hole-injection layers (HILs) and/or hole-transport layers (HTLs), light-emitting layers (EMLs), and electron-transport layers (ETLs) are necessary for high efficiency, where these layers can be optimized, respectively, according to their functions.[1–3] For LEDs based on small molecules, it is rather straightforward to adopt this multilayer strategy via layer-by-layer vacuum deposition. However, for polymer-based LEDs, where solution-based casting or spin-coating is the basic way to form films, it is very challenging to form multilayer structures, because of solvent erosion of previously deposited layers during spin-coating.[4] To overcome this problem, a crosslinkable HTL has been developed for fabricating high-efficiency LEDs, such as those based on fluorescent conjugated polymers and red phosphorescent emitters.[5–9]

For blue LEDs, because most of the blue phosphorescent emitters possess quite high energy levels at their highest occupied molecular orbital (HOMO) (for example, the HOMO for bis(4′,6′-difluorophenylpyridinato) tetrakis(1-pyrazolyl)-borate (FIr6) is –6.1 eV), it is quite difficult to obtain efficient hole injection. In order to alleviate this problem, crosslinkable tetraphenylbiphenyldiamine (TPD, HOMO level at –5.3 eV) and tris(4-carbazole)triphenylamine (TCTA, HOMO level at –5.7 eV) have been developed to provide cascade hole injection and transport, in order to achieve high efficiency.[10]

For white organic LEDs (WOLEDs), high power efficiency (PE) is the most important criteria for achieving low power consumption. In the case of small-molecule-based devices, it has been reported that p-type doping at the anode side to form HILs and n-type doping at the cathode side to form electron-injection layers (EILs) can significantly decrease the driving voltage and increase the PE.[11–13] To avoid quenching of luminescence by these doped layers, a neutral HTL (ca. 10 nm) is often deposited as a spacer between the p-doped HTL and the EML, whereas an electron-transporting spacer (ca. 10 nm) is deposited between the ETL and EML.[14] The commercially available PEDOT:PSS (Bayer Inc.), a conductive polymer blend that is composed of poly(3,4-ethylenedioxythiophene) doped with poly(styrene sulfonic acid), has been widely used as a HIL for polymer LEDs (PLEDs) because of its good electrical, optical, and mechanical properties.[15,16] To avoid quenching of the EML, a semiconducting polymer interlayer (ca. 10 nm) was inserted between the PEDOT:PSS layer and the EML, and all these layers were formed via spin-coating.[17] The interlayer on top of the PEDOT:PSS layer was also annealed at 180 °C, a temperature higher than its glass-transition temperature (T_g), for one hour to gain solvent resistance, although the mechanism was not clearly explained. Very recently, a poly(vinyl carbazole) (PVK)-based ethanol-soluble polyelectrolyte (sulfonated with lithium salt) was used as an HTL on top of the PEDOT:PSS layer. The EML can then be formed via spin-coating from a solution using a nonerosive solvent.[18] By using another electron-transporting polyelectrolyte (sulfonated with sodium salt) as the ETL, and blends of blue- and green-emitting conjugated polymers with an orange-emitting iridium complex as the EML, promising WOLEDs were demonstrated with PEs of ca. 3 lm W^{-1} (1 lm = 1 cd sr^{-1}), measured in the forward direction (ca. 6 lm W^{-1} if the emission from all directions was included).

In this communication, we report the realization of high-efficiency polymer WOLEDs using a hole-injection/transport bilayer that can be formed by thermally crosslinking a TCTA-based HTL on top of a PEDOT:PSS layer. Integrating a conductive HIL and a crosslinkable HTL together resulted in a low driving voltage, cascade hole injection, and effective electron blocking/exciton confinement in the fabricated LEDs. This also translates into devices with high quantum efficiency and PE. A PE of ca. 5.6 lm W^{-1} at a forward brightness of 800 Cd m^{-2} was achieved for WOLEDs with phosphorescent emitters doped with PVK. The device emitted white color in the entire driving-voltage span with the Commission Interna-

[*] Prof. A. K.-Y. Jen, Dr. Y.-H. Niu, Dr. M. S. Liu, Dr. J.-W. Ka, J. Bardeker, M. T. Zin, R. Schofield
Department of Materials Science and Engineering
University of Washington
Box 352120, Seattle, WA 98195 (USA)
E-mail: ajen@u.washington.edu
Prof. Y. Chi
Department of Chemistry
National Tsing Hua University
Hsin Chu 300 (Taiwan)

[**] This work was supported by the National Science Foundation's NSF-STC program under DMR-0120967 and the University of Washington through the Technology Gap Innovation Fund.

tionale de I'Eclairage (CIE) coordinates from (0.379,0.367) to (0.328,0.351), which were very close to the white standards, (0.333,0.333).

As shown in Scheme 1, a TCTA derivative with two crosslinkable vinylbenzyl (VB) ether groups was synthesized. It has been reported that the double bond on the VB ether groups could be polymerized neat at a temperature above 150 °C.[19,20] As was shown in the differential scanning calorimetry (DSC) measurement of VB-TCTA (inset of Fig. 1a), the pristine VB-TCTA exhibited a T_g of around 80 °C, which is much lower than that of the pure TCTA. It also showed an exothermic peak at 170 °C, which corresponds to the crosslinking process. After isothermal heating at 180 °C for 30 min, the sample was slowly cooled to room temperature and then re-scanned. A broad transition with T_g centered at ca. 175 °C was detected from the second ramp, indicating that the crosslinked segments might have varied length scales. Meanwhile, no apparent exothermal peak appeared until 250 °C, indicating that the VB-TCTA was completely crosslinked. Consistent with this observation, good solvent resistance was achieved for films cured at 180 °C for 30 min (Fig. 1b). The UV-vis absorbance of the freshly cured film remained the same after being washed with chlorobenzene, a solvent that is used for spin-coating EMLs. Contrastingly, if the film was only cured at 160 °C for 30 min, it did not reach the needed solvent resistance, as shown in Figure 1a. Therefore, the typical crosslinking conditions used for device fabrication were 180 °C for 30 min.

By spin-coating from the solution of VB-TCTA in 1,2-dichloroethane, uniform films could be formed on top of the predried (125 °C for 10 min) PEDOT:PSS layer.[21] After being thermally cured at 180 °C for 30 min, the films retained a mirrorlike smoothness. The morphology of a cured film of VB-TCTA with nominal thickness of 15 nm is shown in the inset of Figure 1b. The root-mean-square (RMS) surface roughness of the film was 1.24 nm, which is smaller than that of the two controls on indium tin oxide (ITO) (1.41 nm for the PEDOT:PSS film thermally treated at 125 °C for 10 min, and 1.49 nm for the one treated at 180 °C for 30 min).[22]

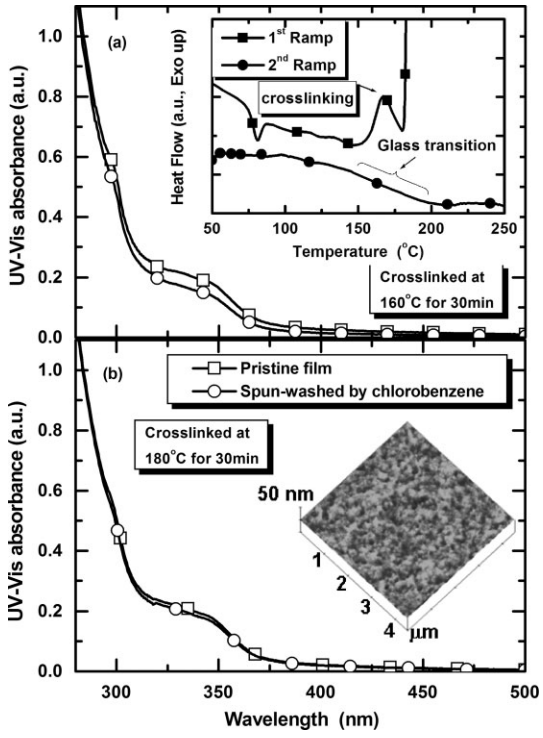

Figure 1. UV-vis absorbance of the VB-TCTA films that were partly crosslinked at 160 °C for 30 min (a) or fully crosslinked at 180 °C for 30 min (b). Pristine crosslinked films (□) in comparison with those spin-washed by chlorobenzene (○). The inset of (a) shows the DSC measurement of VB-TCTA. From the first ramp to the pristine VB-TCTA, it can be clearly seen that the thermal crosslinking process begins around 150 °C and peaks at 170 °C. After isothermal heating for 30 min at 180 °C, the sample was cooled to room temperature to begin the second ramp. The ramp rate was 10 °C min^{-1} in both scans. The inset of (b) shows the surface morphology of the crosslinked (180 °C for 30 min) VB-TCTA film on top of a layer of PEDOT:PSS on indium tin oxide (ITO).

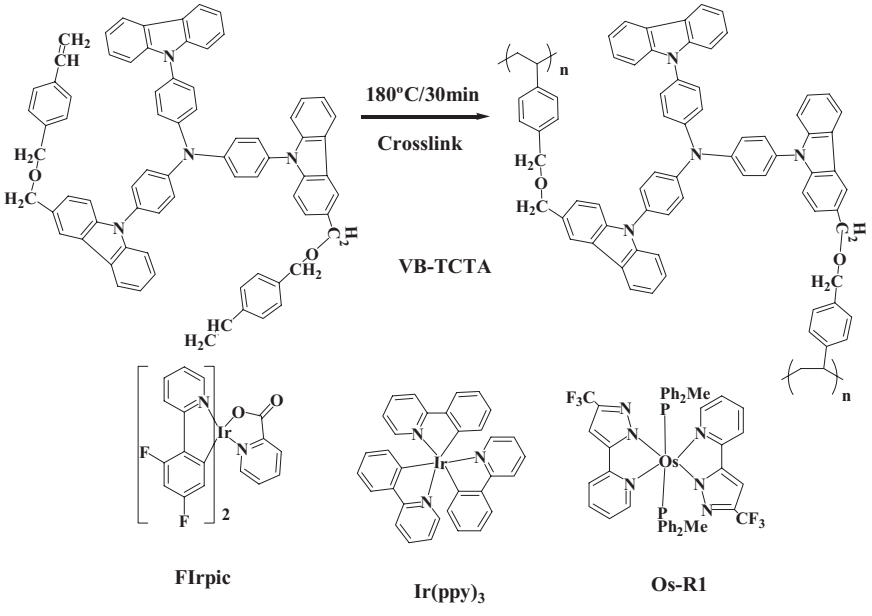

Scheme 1. Chemical structures of the related materials and the structural change of VB-TCTA after crosslinking.

To understand the surface-element distribution of the resultant films, measurements from X-ray photoelectron spectroscopy (XPS) were conducted on both PEDOT:PSS and PEDOT:PSS/crosslinked VB-TCTA bilayer films with different VB-TCTA-coverage thickness. As shown in Figure 2a, the relative surface atomic concentrations of C, O, S, and Na were quantitatively calculated from their C 1s, O 1s, S 2p, and Na 1s peaks. Their variations with

ADVANCED MATERIALS

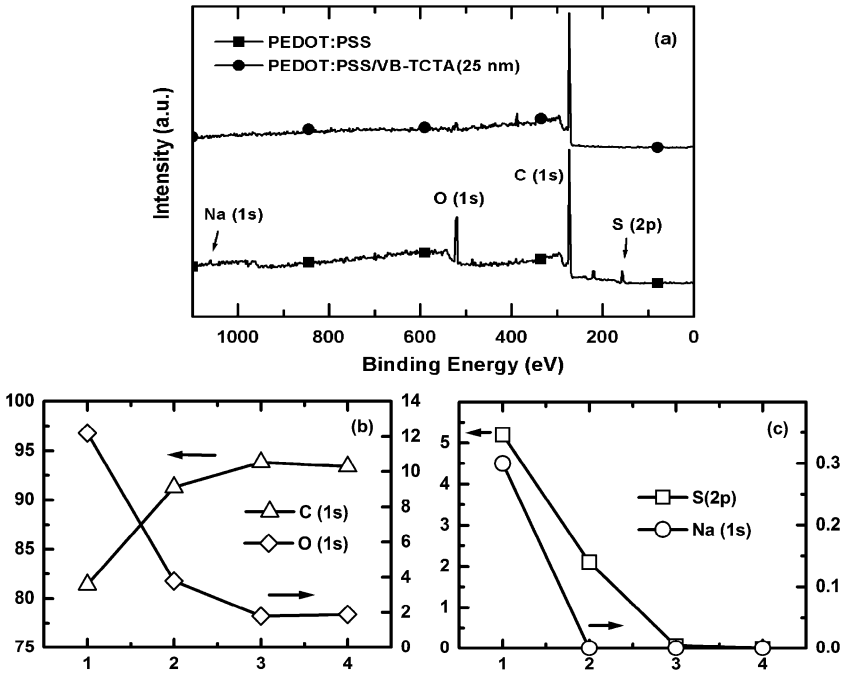

Figure 2. a) XPS spectrum of a representative VB-TCTA film on top of a layer of PEDOT:PSS on ITO compared to that of the PEDOT:PSS. The VB-TCTA film was crosslinked at 180 °C for 30 min. b,c) Variation of the relative surface atomic concentrations that were averaged from three-spot test results. On the *x*-axis of (b) and (c): **1** corresponds to PEDOT:PSS film; **2** to PEDOT:PSS/VB-TCTA (15 nm); **3** to PEDOT:PSS/VB-TCTA (25 nm); and **4** to PEDOT:PSS/VB-TCTA (34 nm). All the films were thermally cured at 180 °C for 30 min on a hotplate in an argon-protected glove-box.

different VB-TCTA thicknesses are shown in Figure 2b and c, where the values were averaged from three spots from high-definition scans of these peaks. Interestingly, the signals from the S and Na elements, which only existed in the PEDOT:PSS layers, decreased dramatically as the thickness of VB-TCTA increased. The signal from Na disappeared completely from the surface when the VB-TCTA thickness was greater than 15 nm, however, the signal from S remained and it only decreased to about half of the S intensity of the PEDOT:PSS film. This indicates either that the PSS chains penetrated into the VB-TCTA layer during its spin-coating and/or crosslinking processes, or that some of the VB-TCTA molecules penetrated into the voids of the PSS's abundant surface and then crosslinked in situ. Nevertheless, the signal from S disappeared completely when the thickness of VB-TCTA was further increased to 25 nm. At the present time, it is difficult to judge whether a bicontinuous interpenetrating network (IPN) structure or simply some surface mixing between the PSS chain and the in situ crosslinked VB-TCTA was formed near the interface region.[23,24] However, the crosslinked VB-TCTA above this interfacial region could also function as a spacer to prevent the PEDOT:PSS chain and other mobile constituents from penetrating into the EML and quenching the emission.

The EML was formed by spin-coating a blended solution of 79 wt % PVK as host,[25] 20 wt % FIrpic as blue emitter,[26] 0.5 wt % $Ir(ppy)_3$ as green emitter,[27] and 0.5 wt % Os-R1 as red emitter[28] in chlorobenzene on top of the ITO/PEDOT:PSS/crosslinked VB-TCTA substrates, with varied VB-TCTA thicknesses of 15, 25, and 34 nm. The LEDs fabricated are hereafter called device **2**, **3**, and **4**, respectively. The PEDOT:PPS-only device is called device **1**. The chemical structures of each component are shown in Scheme 1 and their energy levels are shown in Scheme 2. It is well documented that the dominant mechanism for forming excitons in a doped system is through direct charge-carrier trapping and recombination.[29] For this multicomponent doped system, energy transfer from the blue emitter to the green and the red is also quite possible.[30] As shown in Figure 3a and Table 1, the turn-on voltage of control device **1** was 5.2 V, the maximum external quantum efficiency (η_{ext}) was 2.07 %, and the PE was 2.08 lm W^{-1} at a forward brightness of 800 Cd m^{-2}. These values are quite similar to a previously reported blend system.[25] For devices **2** and **3**, the turn-on voltage decreased to 4.8 V, showing the effect of the lowered hole-injection barriers through cascade injection.[10] As shown in Figure 3b and Table 1, all the devices with VB-TCTA

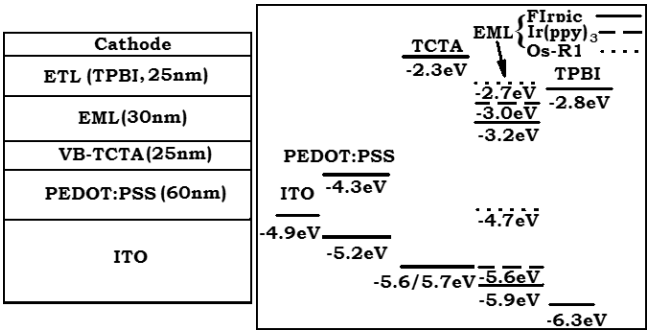

Scheme 2. Device structure and energy-level diagrams.

layers showed roughly twice (or higher) the efficiency of the PEDOT:PSS-only control device, indicating a more balanced carrier injection and recombination. This should be attributed to enhanced hole injection via cascade hopping and effective electron blocking at the EML/VB-TCTA interface, because the lowest unoccupied molecular orbit (LUMO) level of TCTA lies at –2.3 eV.[31,32] Better exciton confinement could also be achieved because the bandgap of TCTA (3.3–3.4 eV) is much larger than the exciton energies of the emitters in the EML. The best performance achieved from device **3** gave a maximum η_{ext} of 5.85 %, a PE of 6.15 lm W^{-1}, and a luminosity efficiency (LE) of 10.9 Cd A^{-1}. The PE remained quite high (5.59 lm W^{-1}) at a forward brightness of 800 Cd m^{-2}. For

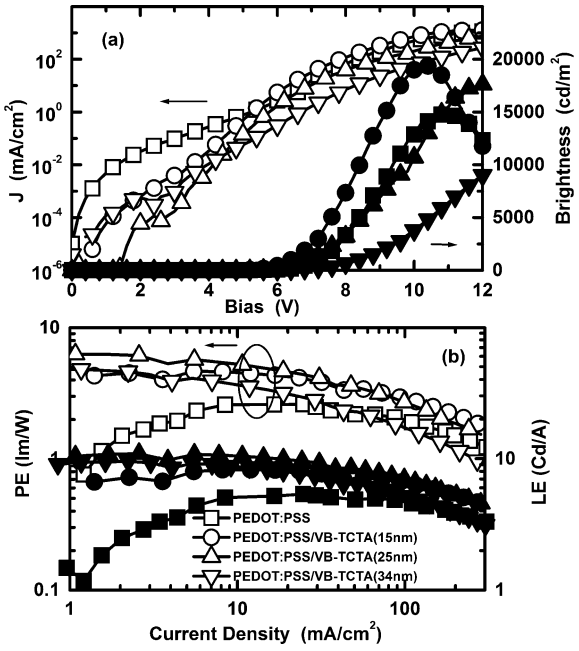

Figure 3. a) Current density–voltage (*J–V*, open symbols) and brightness–voltage (*B–V*, solid symbols) characteristics. b) PE (open symbols) and luminosity efficiency (solid symbols) variations versus *J* of the WOLEDs with different anode hole-injection/hole-transport constituents.

Table 1. Device performance recorded from the normal direction of the anode side. Device structure: ITO/PEDOT:PSS (60 nm)/HTL/blend of FIrpic, $Ir(ppy)_3$, and Os-R1 in PVK (30 nm)/ tris(*N*-phenylbenzimidazol-2-yl)benzene TPBI (25 nm)/CsF (1 nm)/Al (200 nm).

HTL	None	VB-TCTA thickness		
		15 nm	25 nm	34 nm
1evice no.	**1**	**2**	**3**	**4**
Turn-on voltage [V]	5.2	4.8	4.8	5.6
Maximum η_{ext} [photons	2.07	4.01	5.85	5.20
electron^{-1} %] with PE[a]/LE[b]	2.09/4.30	4.64/8.23	6.15/10.9	4.63/9.54
Maximum brightness [cd m-$^{-2}$]	11,900	19,380	17,630	10,860
at driving voltage [V]	11.0	10.2	12.0	13.6
PE[a] at 800 cd m^{-2}	2.08	4.56	5.59	3.74

[a] PE in lm W^{-1}. [b] Luminous in cd A^{-1}.

device **4**, which had a thicker VB-TCTA layer, the turn-on voltage increased to 5.6 V and the device performance also decreased, possibly because of mismatched low hole mobility in VB-TCTA compared with that in PEDOT:PSS.

Figure 4 shows the electroluminescence (EL) spectra measured from device **3** at different driving voltages. Good color stability versus driving voltage could be achieved with CIE coordinates varying from (0.379,0.367) at 6 V to (0.328,0.351) at 12 V, which are both very close to the standard for pure white. The slight increase of blue emission at elevated voltages reflects certain preferential saturation of the limited amount of low-energy emitters in the blend.[33]

For general lighting applications, one should count all the light emitted from the device. According to the estimation

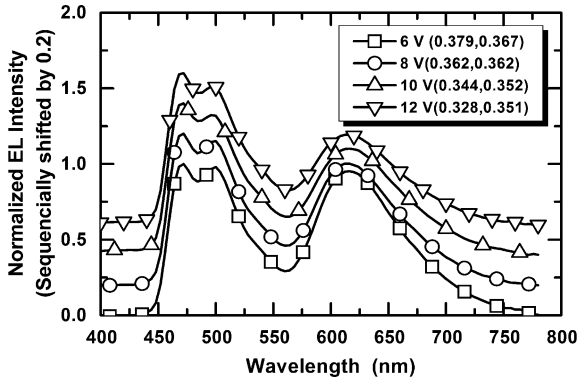

Figure 4. EL spectra and corresponding CIE coordinates at different driving voltages for the LED with PEDOT:PSS/VB-TCTA(25 nm) bilayer HIL/HTL structure. The spectra are vertically shifted for clarity.

from Gong et al. and Forrest and co-workers,[18,30] a factor of ca. 2 should be applied to the value of the corresponding forward-viewing external efficiency in order to get the total LE and PE. If we take this into account, a PE value of more than 11 lm W^{-1} could be realized for device **3** at a forward brightness of 800 Cd m^{-2}, which is very respectable for the polymer-based WOLEDs.[2,18]

In conclusion, high-efficiency polymer WOLEDs were demonstrated by using a hole-injection/transport bilayer that was formed by thermally crosslinking a TCTA-based HTL on top of a PEDOT:PSS layer. The excellent solvent resistance of the fully crosslinked HTL ensured the subsequent solution processing of the EML. A possible surface-mixing structure formed at the interface between the HIL and HTL facilitated cascade hole injection and lowered the driving voltage, whereas the upper crosslinked pure VB-TCTA part functioned as an electron-blocking/exciton-confinement layer and thereby helped prevent quenching of the EML. High power efficiency (ca. 5.6 lm W^{-1} for the forward emission or > 11 lm W^{-1} when all the light emitted from the device is included) can be achieved at a forward brightness of 800 Cd m^{-2}. The device also emitted quite stable white light with the CIE coordinates varying from (0.379,0.367) to (0.328,0.351), which are very close to those of the white standard (0.333,0.333).

Experimental

Synthesis: TCTA was prepared employing an Ullmann reaction between tris(4-iodo)triphenylamine and carbazole in the presence of copper and potassium carbonate. The formyl groups were introduced into TCTA through a Vilsmeier reaction with excess amounts of *N,N′*-dimethylformamide (DMF) and phosphorus oxychloride ($POCl_3$). The further reduction of the TCTA dialdehyde gave a large yield of bishydoxy-containing TCTA. The reaction of hydroxy-functionalized TCTA with 4-vinylbenzyl chloride using sodium hydride as the dehydration reagent gave bisvinylbenzyl ether-containing TCTA (VB-TCTA).

Device Fabrication: The HTL was formed by spin-coating solutions of VB-TCTA in 1,2-dichloroethane on top of a predried (125 °C for 10 min) PEDOT:PSS layer. After being fully crosslinked at 180 °C for

ADVANCED MATERIALS

30 min, the EL layer with a thickness of around 30 nm was spin-coated on top of the HIL/HTL bilayer. In a vacuum below 1×10^{-6} Torr (1 Torr ≈ 133 Pa), the ETL, composed of 1,3,5-tris(*N*-phenylbenzimidazol-2-yl)benzene (TPBI, ca. 25 nm), was sublimed. Cesium fluoride with a thickness of 1 nm and aluminum with a thickness of 200 nm were subsequently evaporated to form the cathode [34].

Performance Measurement: The device testing was carried out in air at room temperature. EL spectra were recorded by an Oriel Instaspec IV spectrometer with a CCD detector. Current–voltage (*I–V*) characteristics were measured on a Hewlett Packard 4155B semiconductor parameter analyzer. The power of the EL emission in the normal direction of the ITO side was measured using a calibrated Si-photodiode and a Newport 2835-C multifunctional optical meter. The relationship of the forward brightness and efficiencies were calculated from the forward output power together with the EL spectra of the devices, under the assumption that the emission followed a Lambertian space distribution [35]. Forward emission LE and PE thereafter were recalibrated with a directly measured brightness–current-density relationship by a PR-650 SpectraColorimeter (Photo Research Co.). The CIE coordinates were measured with the PR-650 at the same time.

Atomic Force Microscopy (AFM) and XPS Characterizations: For reliable comparison, one piece of PEDOT:PSS on ITO was sliced into four and VB-TCTA layers with different thicknesses were then formed on them via spin-coating and thermal annealing, respectively. Tapping-mode measurements in air were made using a Nanoscope III AFM device (Digital Instruments). XPS measurements were made at the standard analysis angle (35°) using an X-Probe (Surface Sciences Instruments) with an Al Kα source in a vacuum chamber at pressures of ca. 5×10^{-9} Torr.

Received: December 30, 2006
Revised: August 3, 2006
Published online: January 3, 2007

[1] J. H. Burroughes, D. D. C. Bradley, A. R. Brown, R. N. Marks, K. Mackay, R. H. Friend, P. L. Burns, A. B. Holmes, *Nature* **1990**, *347*, 539.
[2] B. W. D'Andrade, S. R. Forrest, *Adv. Mater.* **2004**, *16*, 1585.
[3] J. R. Sheats, *Science* **1997**, *277*, 191.
[4] H. Yan, B. J. Scott, Q. Huang, T. Marks, *Adv. Mater.* **2004**, *16*, 1948.
[5] S. Liu, X. Jiang, H. Ma, M. S. Liu, A. K.-Y. Jen, *Macromolecules* **2000**, *33*, 3514.
[6] X. Jiang, S. Liu, H. Ma, A. K.-Y. Jen, *Appl. Phys. Lett.* **2000**, *76*, 1813.
[7] X. Jiang, S. Liu, M. S. Liu, P. Herguth, A. K.-Y. Jen, H. Fong, M. Sarikaya, *Adv. Funct. Mater.* **2002**, *12*, 745.
[8] H. Yan, P. Lee, N. R. Armstrong, A. Graham, G. A. Evmenenko, P. Dutta, T. Marks, *J. Am. Chem. Soc.* **2005**, *127*, 3172.
[9] Y.-H. Niu, B. Chen, S. Liu, H. Yip, J. Bardecker, A. K.-Y. Jen, J. Kavitha, Y. Chi, C.-F. Shu, Y.-H. Tseng, C.-H. Chien, *Appl. Phys. Lett.* **2004**, *85*, 1619.
[10] Y.-H. Niu, M. S. Liu, J.-W. Ka, Alex K.-Y. Jen, *Appl. Phys. Lett.* **2006**, *88*, 093 505.
[11] X. Zhou, J. Blochwitz, M. Pfeiffer, A. Nollau, T. Fritz, K. Leo, *Adv. Funct. Mater.* **2001**, *11*, 310.
[12] W. Guo, A. Kahn, *J. Appl. Phys.* **2003**, *94*, 359.
[13] A. G. Werner, F. Li, K. Harada, M. Pfeiffer, T. Fritz, K. Leo, *Appl. Phys. Lett.* **2003**, *82*, 4495.
[14] G. He, O. Schneider, D. Qin, X. Zhou, M. Pfeiffer, K. Leo, *J. Appl. Phys.* **2004**, *95*, 5773.
[15] Y. Cao, G. Yu, C. Zhang, R. Menon, A. J. Heeger, *Synth. Met.* **1997**, *87*, 171.
[16] A. Berntsen, Y. Croonen, C. Liedenbaum, H. Schoo, R.-J. Visser, J. Vleggaar, P. van de Weijer, *Opt. Mater.* **1998**, *9*, 125.
[17] J.-S. Kim, R. H. Friend, I. Grizzi, J. H. Burroughes, *Appl. Phys. Lett.* **2005**, *87*, 023 506.
[18] X. Gong, S. Wang, D. Moses, G. C. Bazan, A. J. Heeger, *Adv. Mater.* **2005**, *17*, 2053.
[19] F. R. Mayo, *J. Am. Chem. Soc.* **1968**, *90*, 1289.
[20] N. Teramoto, M. Shibata, *J. Appl. Polym. Sci.* **2004**, *91*, 46.
[21] L. D. Bozano, K. R. Carter, V. Y. Lee, R. D. Miller, R. DiPietro, J. C. Scott, *J. Appl. Phys.* **2003**, *94*, 3061.
[22] J. Huang, P. F. Miller, J. S. Wilson, A. J. de Mello, J. C. de Mello, D. D. C. Bradley, *Adv. Funct. Mater.* **2005**, *15*, 290.
[23] H. Peisert, M. Knupfer, F. Zhang, A. Petr, L. Dunsch, J. Fink, *Appl. Phys. Lett.* **2003**, *83*, 3930.
[24] L. H. Sperling, *Interpenetrating Polymer Networks and Related Materials*, Plenum, New York **1981**, Ch. 1.
[25] Y. Kawamura, S. Yanagida, S. R. Forrest, *J. Appl. Phys.* **2002**, *92*, 87.
[26] C. Adachi, R. C. Kwong, P. Djurovich, V. Adamovich, M. A. Baldo, M. E. Thompson, S. R. Forrest, *Appl. Phys. Lett.* **2001**, *79*, 2082.
[27] C. Adachi, M. A. Baldo, S. R. Forrest, M. E. Thompson, *Appl. Phys. Lett.* **2000**, *77*, 904.
[28] Y.-L. Tung, P.-C. Wu, C.-S. Liu, Y. Chi, J.-K. Yu, Y.-H. Hu, P.-T. Chou, S.-M. Peng, G.-H. Lee, Y. Tao, A. J. Carty, C.-F. Shu, F.-I. Wu, *Organometallics* **2004**, *23*, 3745.
[29] X. Gong, J. C. Ostrowski, D. Moses, G. C. Bazan, A. J. Heeger, *Adv. Funct. Mater.* **2003**, *13*, 439.
[30] B. W. D'Andrade, R. J. Holmes, S. R. Forrest, *Adv. Mater.* **2004**, *16*, 624.
[31] Y. Kuwabara, H. Ogawa, H. Inada, N. Noma, Y. Shirota, *Adv. Mater.* **1994**, *6*, 677.
[32] R. J. Holmes, B. W. D'Andrade, S. R. Forrest, X. Ren, J. Li, M. E. Thompson, *Appl. Phys. Lett.* **2003**, *83*, 3818.
[33] G. Li, J. Shinar, *Appl. Phys. Lett.* **2003**, *83*, 5359.
[34] T. M. Brown, R. H. Friend, I. S. Millard, D. J. Lacey, J. H. Burroughes, F. Cacialli, *Appl. Phys. Lett.* **2001**, *79*, 174.
[35] N. C. Greenham, R. H. Friend, D. D. C. Bradley, *Adv. Mater.* **1994**, *6*, 491.

